Journal of Power Sources 196 (2011) 1314–1320

Contents lists available at ScienceDirect

Journal of Power Sources

journal homepage: www.elsevier.com/locate/jpowsour

Effect of gas diffusion layer anisotropy on mechanical stresses in a polymer electrolyte membrane

Mustafa Fazil Serincan*, Ugur Pasaogullari

Department of Mechanical Engineering, and Center for Clean Energy Engineering, University of Connecticut, 44 Weaver Rd Unit 5233, Storrs, CT 06269, USA

ARTICLE INFO

Article history:
Received 12 April 2010
Accepted 11 June 2010
Available online 18 June 2010

Keywords:
Fuel cell
Membrane
Stress
Swelling
Anisotropy
Gas diffusion layer (GDL)

ABSTRACT

Mechanical stresses arise in a polymer electrolyte fuel cell (PEFC) components since the polymer electrolyte membrane swells and shrinks with the change in hydration and these dimensional changes of the membrane are constrained by the cell assembly and the gas diffusion layers (GDLs). The carbon paper that is used as the GDL in PEFCs exhibits strong anisotropy due to the orientation of the fibers in the material. In this study, we investigate the role of GDL anisotropy on the stress distribution in a PEFC. A finite element model is developed to determine the mechanical stresses in a PEFC membrane. The impact of GDL anisotropy on the mechanical stresses in the membrane is emphasized and it is shown that isotropic mechanical properties lead to inaccurate stress predictions. Due to very low Young's modulus of the GDL in the through-plane direction (0.5 MPa) compared to its in-plane value (9 GPa), through-plane stresses induced in the membrane become negligible. The effects of the water content profiles on the stress distribution are also investigated and it is found that accurate description of water transport is critical for a reliable analysis of the hygral stresses.

1. Introduction

Due to their low pollutant emissions and high power densities, polymer electrolyte fuel cells (PEFCs) are among the prominent candidates for the alternative power generation method of the near future. PEFCs are currently being developed for applications in busses, automobiles and boats, and their potential for use in stationary applications is gradually increasing.

Although very promising electrochemical performance has been reported under wide range of conditions, the reliability and durability of the cells remains as one of the most challenging hurdles to be tackled for the successful deployment of the PEMFC technology. PEFCs are required to resist permanent changes in performance over time, tolerate unexpected changes in the ambient conditions and continue a stable operation, and sustain a structural integrity under various operating conditions. However, during the operation, a PEFC is prone to many hazards that may cause degradation of the performance to the extent of complete failure of the cell.

Degradation of the PEFCs can be studied under two main sections: electrochemical degradation and mechanical degradation, which are generally coupled. Electrochemical degradation can be due to various factors such as air and fuel impurities poisoning the catalyst sites and the membrane, dissolution, migration and agglomeration of platinum causing a decrease in the electrochemically active area. Electrochemical degradation of the PEFCs takes a great attention from the researchers and reported studies to characterize the degradation mechanisms are abundant for which we refer to the comprehensive review paper of Rama et al. on the degradation and failure of the PEFCs [1]. On the other hand, most common causes for mechanical degradation of a PEFC can be summarized as cyclic cell operation with or without exposure to subzero conditions, inhomogeneous or excessive compression of the cell by the bipolar plates, mechanical shock and vibration due to the operation environment, mechanical stresses induced by thermal hotspots at the regions with high electrical contact resistance, and the mechanical stresses due to swelling of the membrane. It is now well established that even though the chemical degradation causes the decrease in the performance, the mechanical degradation is the primary reason for cell failure, which usually comes up as membrane's losing the ability to separate reactant gases.

Of these factors, effect of mechanical stresses due to swelling of the membrane is not studied as widely as others. There are only a few experimental studies reported to characterize the effects of membrane swelling on cell degradation [2] and to investigate the effects of membrane humidity on the mechanical properties of the membrane [3,4]. There are also numerical studies to investigate the mechanical stresses induced in the materials due to the swelling of the membrane [5–9]. Kusoglu et al. investigated the mechanical response of the fuel cell subjected to a single hygro-thermal duty

* Corresponding author at: UNIDO-ICHET, Sabri Ulker Sok. 38/4 Cevizlibag, Zeytinburnu, 34015 Istanbul, Turkey. Tel.: +90 5325173197; fax: +90 2124168947.
E-mail address: fazil.serincan@engr.uconn.edu (M.F. Serincan).

0378-7753/$ – see front matter © 2010 Elsevier B.V. All rights reserved.
doi:10.1016/j.jpowsour.2010.06.026

Nomenclature

Symbols

c_w	water concentration in the membrane
D	elasticity matrix
E	Young's modulus
G	shear modulus

Greek

β	swelling expansion coefficient
ε	normal strain
γ	shear strain
ν	Poisson's ratio
ρ	density
σ	normal stress
τ	shear stress

Subscripts

0	initial
el	elastic
eq	equilibrium
ref	stress free state

cycle [7]. They predicted that the membrane undergoes a plastic deformation, which can result in cracks and pinholes. In another study by the same group, it is emphasized that the impact of the non-uniform swelling on the fatigue stresses is significant [8].

None of the modeling studies mentioned above has considered the anisotropy in the mechanical properties of the gas diffusion layer (GDL), and we hypothesize that the anisotropy of the GDL has a significant impact on the stress distribution in the membrane. GDL typically consist of carbon fibers aligned parallel to the material surface as seen in Fig. 1. Because of the orientation of the fibers, GDL exhibits a strong anisotropy and the properties such as thermal conductivity and electrical resistance differ significantly in the through-plane (e.g., anode-to-cathode) and in-plane (e.g., channel-to-current collector) directions [10]. Pasaogullari et al. have investigated the anisotropic heat and mass transfer in the gas diffusion layer of a PEMFC and reported that anisotropic nature of the GDL has a significant impact on the temperature and liquid water distribution, consequently [11]. Recently, Kleemann et al. have conducted tests to characterize the anisotropy in mechanical properties of the GDL [12] and reported that the through-plane mechanical properties are significantly different than in-plane properties. The mechanical properties of the GDL are presumed to have a major impact on the stress distribution in the membrane as the main reason for the hygro-thermal stresses induced in the materials is due to the mismatch in the elasticity between different neighboring layers of the PEFC. Consequently, in this study, we investigate the effects of GDL anisotropy on the stress distribution in a PEFC membrane with a numerical model. Moreover, in a companion paper, we study the mechanical stresses during the operation of the fuel cell [13].

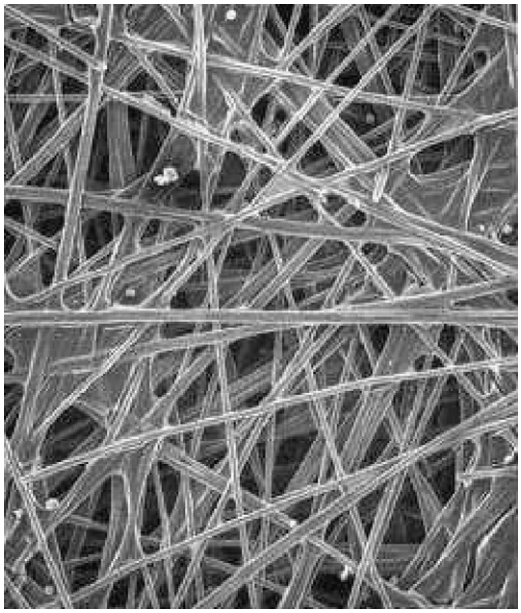

Fig. 1. Surface SEM image of a Toray TGP-H carbon paper, commonly used as GDL in PEMFCs [10].

2. Model description

The finite element model developed in this study incorporates the constitutive relations for an isotropic membrane and an orthotropic GDL. Orthotropic media is a special form of anisotropic media, where the principal axes of the domain coincide with the principal axes of the coordinate system. Force equilibrium equations in the conservative form are solved in these subdomains to calculate the stresses from the deformation field.

In this study, we use plane strain assumption; that is, the strain in one direction is much less than the strain in the two other orthogonal directions. This assumption is safe because of the high aspect ratio of the fuel cell geometry, i.e. channel length 5 cm and the total thickness of the MEA is 0.5 mm. The model geometry can be seen in Fig. 2.

2.1. Constitutive relations

It is assumed that GDL and the membrane undergo linear deformation when subject to hygro-thermal loading. The total strain consists of elastic and hygral strain components:

$$\varepsilon = \varepsilon_{el} + \varepsilon_{sw} \tag{1}$$

With the assumption that hygral expansions are isotropic, the total strain becomes:

$$\varepsilon = \begin{bmatrix} \varepsilon_x \\ \varepsilon_y \\ 0 \\ \gamma_{xy} \end{bmatrix} + \begin{bmatrix} \varepsilon_{sw} \\ \varepsilon_{sw} \\ \varepsilon_{sw} \\ 0 \end{bmatrix} \tag{2}$$

Hygral strain in normal directions is calculated as:

$$\varepsilon_{sw} = \beta(c_w - c_{w,ref}) \tag{3}$$

where β is the membrane swelling expansion coefficient (SEC) defined as change in length for 1% change in relative humidity. c_w is the water content while $c_{w,ref}$ is the value for stress free states (i.e. zero stress state) for hygral expansion. In the simulations, we assume that prior to assembly, Nafion®112 membrane is initially hydrated at 30% relative humidity at room temperature, which corresponds to the stress free state for hygral expansion.

Stress–strain relationship for a linear elastic material is given by:

$$\sigma = D\varepsilon_{el} \tag{4}$$

which can be rewritten using Eq. (1) as:

$$\sigma = D(\varepsilon - \varepsilon_{sw} - \varepsilon_0) \tag{5}$$

Components of σ are σ_x, σ_y, σ_z, τ_{xy} which are the normal and the shear stresses. In our model we model the GDL as an orthotropic

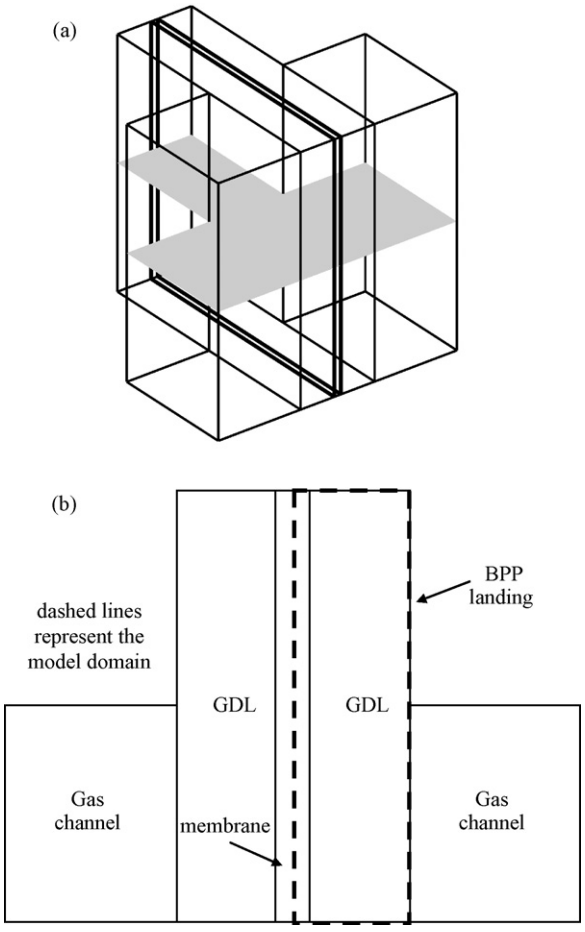

Fig. 2. (a) 3D fuel cell geometry. Shaded cross-section is the 2D model geometry. (b) Finite element model subdomains are shown on the cross-sectional view.

material and the membrane is assumed to be isotropic. For an isotropic material the compliance matrix, the inverse of D, is defined as:

$$D^{-1} = \frac{1}{E}\begin{bmatrix} 1 & -\nu & -\nu & 0 \\ -\nu & 1 & -\nu & 0 \\ -\nu & -\nu & 1 & 0 \\ 0 & 0 & 0 & 2(1+\nu) \end{bmatrix} \quad (6)$$

where E is the Young's modulus and ν is the Poisson's ratio of the material. On the other hand, for an orthotropic material the compliance matrix is defined as:

$$D^{-1} = \begin{bmatrix} 1/E_x & -\nu_{xy}/E_y & -\nu_{zy}/E_z & 0 \\ -\nu_{xy}/E_x & 1/E_y & -\nu_{yz}/E_z & 0 \\ -\nu_{zy}/E_x & -\nu_{yz}/E_y & 1/E_z & 0 \\ 0 & 0 & 0 & 1/G_{xy} \end{bmatrix} \quad (7)$$

where E needs to be known in three normal directions and ν and G, the shear modulus, need to be determined in three different shear planes. Unlike in the case of isotropic materials, these three moduli are not coupled and shear modulus has to be determined separately. However, considering the morphology of the carbon fiber GDLs, it is seen that the fibers are aligned parallel to the material plane but without having an in-plane preferential orientation. Therefore we assume isotropic in-plane (yz plane) properties which implies $E_y = E_z$, $\nu_{xy} = \nu_{xz}$.

Table 1
Material properties.

Gas diffusion layers		
Through-plane Young's modulus (MPa)	$E_x = f(\varepsilon_x)$[a]	[12]
In-plane Young's modulus (MPa)	9000	[12]
Poisson's ratio in xy plane	0	[12]
Poisson's ratio in yz plane	0.25	[10]
Shear modulus in xy plane (MPa)	19.5	[12]
Density (kg m^{-3})	440	[10]
Membrane		
Young's modulus (MPa)	$E = f(\lambda,T)$[a]	[7]
Poisson's ratio	0.25	[14]
Density (kg m^{-3})	1980	[14]
Equivalent weight (EW)	1100	[14]

[a] See the text.

2.2. Material properties

2.2.1. Membrane

Tang et al. determined the swelling strain and Young's modulus of Nafion® 112 as a function of relative humidity and temperature [3]. The polynomial fit to their strain vs. relative humidity data and the Young's modulus values for different relative humidities can be found in Ref. [7]. In our work we relate these properties to the membrane water content, since we predict water content rather than relative humidity in the membrane. A curve fit to the experimental swelling strain data at 85 °C results in:

$$\varepsilon_{sw} = 0.02154 \times \lambda - 0.051846 \quad (8)$$

Another curve fit to their Young's modulus data at 85 °C results in:

$$E = 28.14 \times \exp(3.665\lambda) \quad (9)$$

where Young's modulus is in MPa.

Poisson's ratio of the Nafion 112 is determined from the product data sheet [14]. The values are listed in Table 1.

2.2.2. Gas diffusion layers

The in-plane and through-plane mechanical properties for Toray TGP-H-060 GDL have been investigated by Kleemann et al. [12]. They report the values for through-plane and in-plane Young's moduli (E_x, E_y), Poisson's ratio in the xy plane (ν_{xy}), and the shear modulus in the xy plane (G_{xy}). The values are listed in Table 1 except for E_x, which is not a constant but is given as a function of through-plane strain. Curve fitting to their data, through-plane Young's modulus is expressed as (in MPa):

$$E_x = 89.427 \times {\varepsilon_x}^2 + 2.5816 \times \varepsilon_x + 0.51926 \quad (10)$$

Poisson's ratio in the material plane (ν_{yz}) of the GDL is taken from the product data sheet [10].

2.3. Boundary conditions

The assembly of GDL and membrane is constrained with the bipolar plates (BPP) at both sides. The boundary conditions at the GDL–BPP interfaces are chosen such that motion is constrained in all three directions. This implies that the stack compression materials (i.e. tie rods, bipolar plates and end plates) do not deform under the assembly conditions or during the operation. This is true since the elastic (Young's) modulus of these materials are much higher than the GDL and the membrane. At the GDL–channel interfaces the assembly is assumed to be deforming freely as expected in an actual PEFC assembly. The rest of the boundaries are treated as symmetry planes (Table 2).

Table 2
Geometrical and operational parameters.

Fuel and air channel width	0.5 mm
Land area width	0.5 mm
GDL thickness	0.2 mm
Membrane thickness (Nafion 112)	50.8 μm

3. Results

To analyze the stress distribution in the membrane, we first consider a test case to distinguish the effect of GDL anisotropy. A half-cell model including half of the membrane, and the GDL is investigated with three different GDL properties: (*i*) a less rigid GDL with isotropic properties, (*ii*) a rigid GDL with isotropic properties and (*iii*) an orthotropic GDL with realistic properties. As calculated from Eq. (10), actual GDL, Toray TGP-H-060, has an average through-plane Young's modulus of 0.5 MPa and an in-plane Young's modulus of 9 GPa (case *iii*), as listed in Table 1. For a better comparison, we take the isotropic Young's modulus of the less rigid GDL as 0.5 MPa (case *i*) and the rigid GDL as 9 GPa (case *ii*). We analyze the stress distribution in each case when membrane is subject to swelling due to change in hydration. We consider swelling caused by three different cases: (*i*) under uniform water content profile, i.e. $\lambda = 7$, (*ii*) varying water content along the in-plane direction, i.e. $\lambda = 10$ at the left end (under the bipolar plate landing) of the membrane to $\lambda = 4$ at the right end (under the gas channel) of the membrane, (*iii*) water content changing along the through-plane direction, i.e. $\lambda = 10$ at the membrane–GDL interface to $\lambda = 4$ at the centerline of the membrane.

Fig. 3 shows the deformations in the membrane and GDL as a result of the membrane swelling due to a constant water content profile, i.e. $\lambda = 7$. Recall that the membrane was at a water content of 2.77 during the assembly (corresponding to hydration at 30% relative humidity stress free state). Through-plane displacements (in μm) are plotted on the deformed shape for each case. As expected, the largest deformations occur in the first case of less rigid isotropic GDL for which a maximum displacement of almost 3 μm is observed. Since the motion of the system is restricted by the current collector land of the BPP, the assembly tends to deform through the gas channel, therefore maximum deformations in GDL are seen under the channel areas for all the cases. However, the deformation is observed to be almost uniform in the membrane for case *i* (less rigid isotropic GDL) and for case *iii* (orthotropic GDL). This is because GDL cannot transmit the restriction imposed by the BPP land to the membrane due to the high through-plane elasticity. As a result, the displacements become uniform at the membrane–GDL interface. In case *ii* (rigid isotropic GDL), it is clearly seen that the restriction under the BPP land is transmitted completely to the membrane. Hence half of the membrane corresponding to under the land area barely exhibits any deformations. As a result the displacement is not uniform at the interface but is increasing towards the right half of the membrane, corresponding to under the channel. Although the GDL in case *ii* is much more rigid than the other two, membrane still undergoes a deformation with a maximum through-plane displacement of around 2 μm. However, if the displacement field is averaged over the membrane domain it is seen that the value for rigid GDL (case *ii*) is much lower than that for the other two: 1.46 μm for case *i* and case *iii* and 0.47 μm for case *ii*.

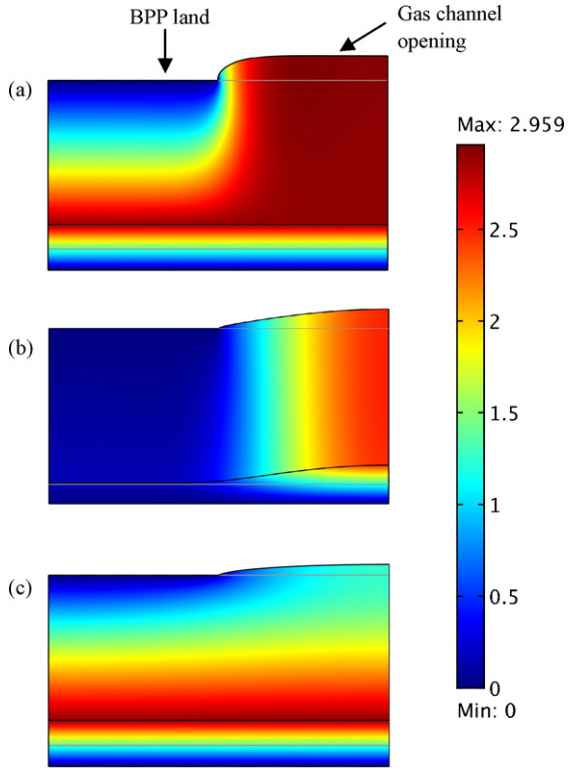

Fig. 3. Displacement fields (in μm) for: (a) less rigid GDL with isotropic properties, $E = 0.5$ MPa, case *i*; (b) rigid GDL with isotropic properties, $E = 9$ GPa, case *ii*; (c) orthotropic GDL with orthotropic properties, $E_{thr} = 0.5$ Mpa and $E_{in} = 9$ GPa, case *iii*. Bottom layer is the membrane and the top layer is the GDL. Deformations are scaled 10 times to be seen clearly in the picture. Gray lines show the undeformed geometry.

Fig. 4 shows in-plane and through stress distributions in the membrane for the same uniform membrane water content. Since all the stresses are in compression, compressive stresses are shown as positive to distinguish the most critical points. The first thing to be noted in all these figures is that the in-plane stresses are much larger than the through-plane stresses. This is expected as the structure can deform more in the through-plane direction. As the membrane tends to swell or shrink, the deformation is restricted by the GDL, which is only partial in the through-plane direction due to free deformation at the channel opening. Since the width of the membrane is much longer compared to its thickness, elongation in the in-plane direction is much less than that in the through-plane direction. (In our model this is implemented as symmetry boundary conditions at the right and left end of the membrane.) Because of these two factors, total strain in the in-plane direction becomes practically zero when the water content is uniform. This also implies that in-plane and out of plane stresses, i.e. along the flow direction (recall Fig. 2 and Eqs. (2), (4) and (6)) are expected to be equal providing that water content is also constant along the flow direction. With these results, it can be concluded that the most critical stresses in the membrane–GDL assembly occur in the material plane. As seen in Fig. 4f, through-plane stresses are practically zero for the orthotropic GDL (case *iii*).

On the other hand, it is seen in Fig. 4 that both in-plane and through-plane stress distributions for case *i* and case *iii* are almost equal. For these two cases through-plane stresses are expected to be very close if not the same because in both cases GDLs have the same through-plane elasticity (5 MPa). However, the in-plane elasticities of two GDLs are quite different: 5 MPa and 9 GPa for case *i* and case *iii*, respectively. The reason why the in-plane stresses are similar can also be attributed to the prediction that the strain in the material plane is practically zero due to not only the potential of the structure to deform freely out through the channel but practically high aspect ratio of the geometry as well. So in order to observe a difference in the in-plane stress distribution for case *i* and case *iii*, there must be a comparable deformation in both directions.

To verify this, we investigate another case when the membrane water content is varying in the in-plane direction such as water content is decreasing linearly from $\lambda = 10$ at the left end of the membrane (under the bipolar plate landing) to $\lambda = 4$ at the right

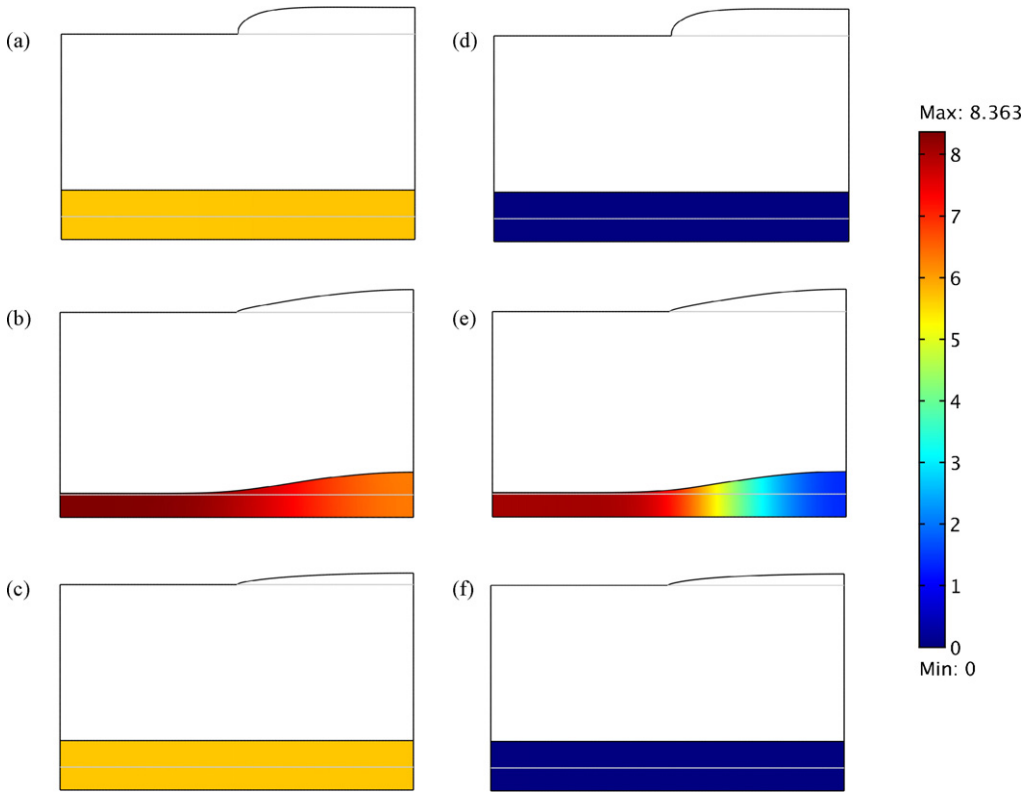

Fig. 4. In-plane *compressive* stress distributions (in MPa) for (a) less rigid isotropic GDL, (b) rigid isotropic GDL, (c) orthotropic GDL, and through-plane *compressive* stress distributions (in MPa) for (d) less rigid isotropic GDL, (e) rigid isotropic GDL and (f) orthotropic GDL. Stress distributions are plotted on the deformed shape where gray lines show the undeformed geometry.

end of the membrane (under the gas channel), similar to – but possibly exaggerated – water distribution in an operating PEFC. Water typically accumulates under the bipolar plate landings due to the larger diffusion distance between the catalyst layer and the channel. The water content profile along the horizontal direction in the membrane can be seen in Fig. 5a.

Fig. 6 shows the deformations in the membrane GDL assembly as a result of the membrane swelling due to the prescribed water content gradient in the in-plane direction. Comparing Fig. 6 with Fig. 3, it is seen that for case *i* and case *iii* the membrane–GDL interface becomes inclined as it is *pulled* upwards from the left end of the membrane. As membrane water content is higher under the BPP areas, those regions tend to swell more than the regions under the channel. As a result the deformation becomes non-uniform at the membrane–GDL interface. For the second case, however, the deformation of the membrane through its thickness is largely restricted by the stiffer GDL. Indeed comparing Figs. 3 and 6 we see a little change in the magnitudes of the displacements for the second case.

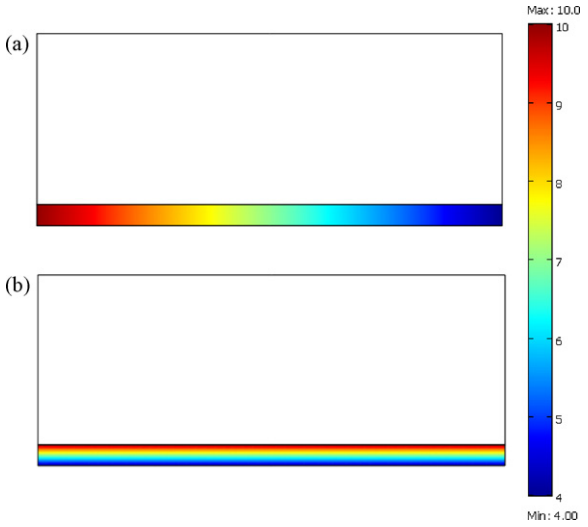

Fig. 5. Membrane water content distributions for (a) in-plane variations and (b) for through-plane variations.

Arrows in Fig. 6 are the displacement vectors and show the direction in which the deformation takes place. According to the arrows shown for case *i*, the structure deforms almost equally in both directions as the arrows show. This is different than case *iii* despite the shapes of the deformed bodies are very similar. This is due to the strong anisotropy of the GDL in the third case. The membrane has isotropic properties, but the large difference between in-plane and through-plane Young's moduli of the GDL affects the deformation of the membrane significantly. As the water content is higher at the left end, the membrane tends to swell without a preferential direction. However, since orthotropic GDL in the third case has a much higher in-plane Young's modulus than that of the membrane, it restricts the in-plane deformation of the membrane. If the in-plane modulus of the GDL was as low 5 MPa (as in case *i*), which indeed is comparable to that for the membrane, the GDL would not pose a significant constraint on the swelling of the membrane in the material plane.

Following the discussions on the membrane's *potential* and *flexibility* to swell, the stress field induced in the membrane can be explained as follows: the deformation of the membrane is confined by the GDL due to the large difference in their material properties, which also means that the GDL is imposing a force on the membrane to restrict its motion. This force results in the compressive stresses induced in the membrane. If for two contiguous layers the

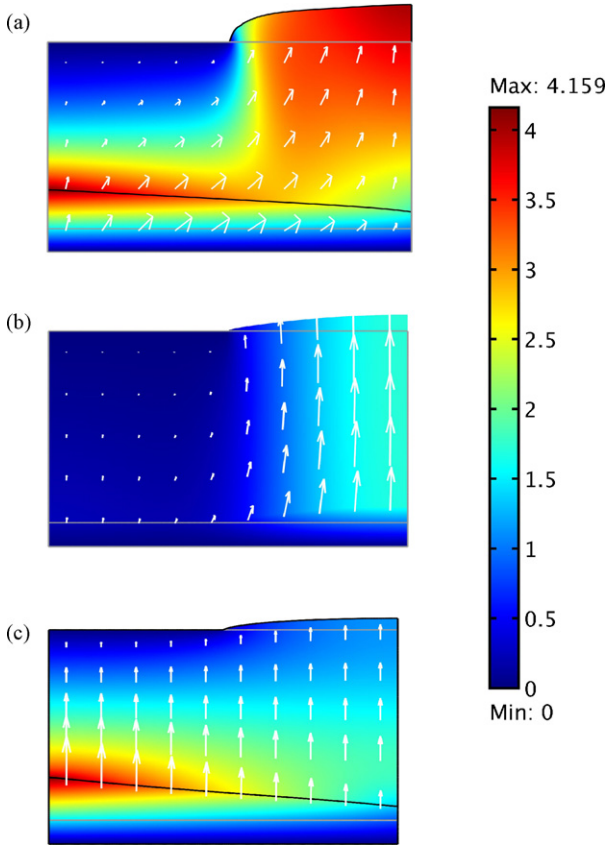

Fig. 6. Through-plane displacement fields (in μm) for the membrane water content varying along in-plane direction from λ = 10 to λ = 4: (a) less rigid isotropic GDL; (b) rigid isotropic GDL; (c) orthotropic GDL. Arrows show the direction of the deformation. Black lines show the interface of the PEM with GDL.

material properties were same, then the composite structure would deform mutually, without one layer causing stresses on the other. Comparing Fig. 7a and c we observe that in-plane stresses for the cases 1 and 3 are quite different. In the first case with the less rigid GDL, the material properties between two layers are comparable. Hence the in-plane stresses induced in the membrane is much less in the first case than the one for the third case with the orthotropic GDL.

Another observation in Fig. 7 is related to the comparison of the stress distributions between case *ii* and case *iii*. Although the in-plane properties of the GDLs are the same for these two cases, the in-plane stresses are much higher in for the one with rigid isotropic GDL (case *ii*), the maximum stress is greater than 13 MPa. In case *ii*, membrane is not only restricted horizontally but also vertically. Another curious observation with Fig. 7b is the variation of the in-plane stresses. As the membrane swells more at the left end (under the bipolar plate landing) where the water content change is higher, larger compressive stresses are induced. As a result, the stress distribution follows the water content distribution.

Although the membrane water content variation discussed recently is similar to what is expected in an operating fuel cell, it is not entirely same as in an operating PEMFC. In an operating PEMFC, there will also be a variation in the water content across the thickness of the membrane due to the water transport between the anode and the cathode. Thus, we also consider the impact of the through-plane variations of the membrane water content on the stress distribution. We investigate a case when the membrane water content is decreasing linearly from λ = 10 at the GDL–membrane interface to λ = 4 at the centerline of the mem-

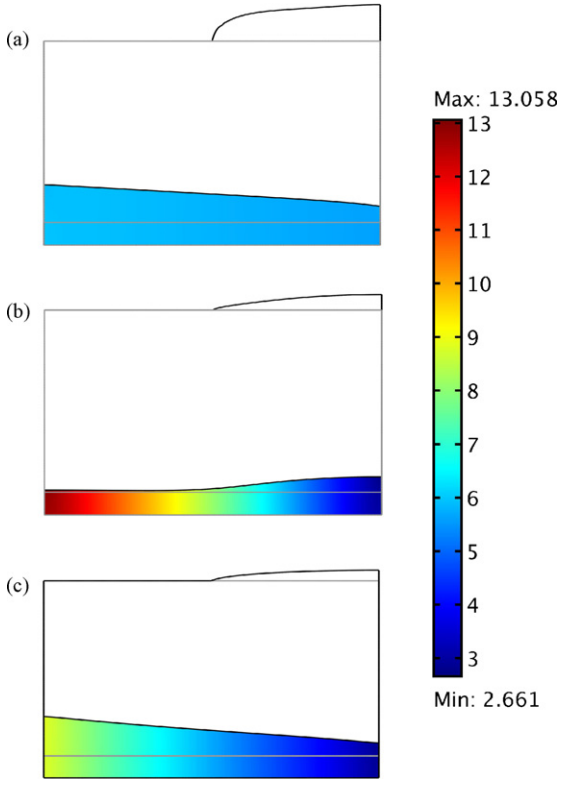

Fig. 7. In-plane compressive stress distributions (in MPa) for the membrane water content varying along in-plane direction from λ = 10 to λ = 4: (a) less rigid isotropic GDL; (b) rigid isotropic GDL; (c) orthotropic GDL.

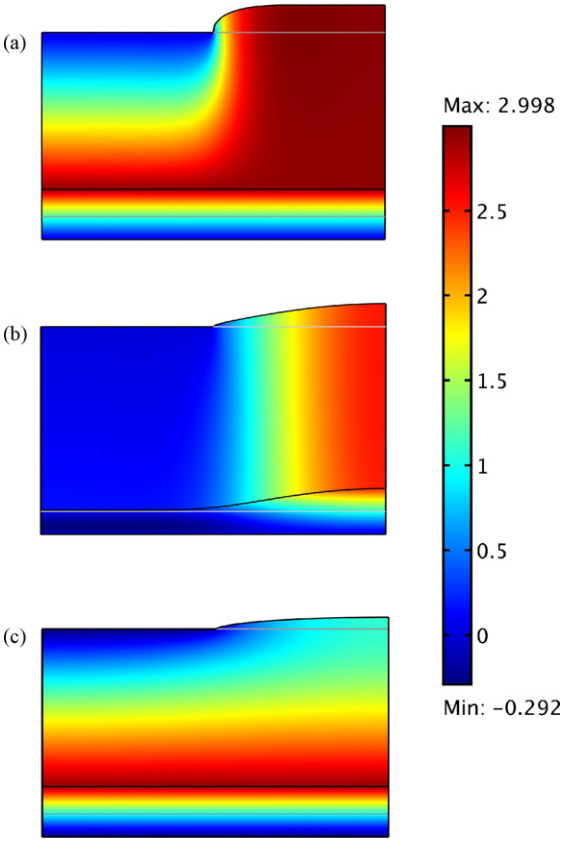

Fig. 8. Displacement fields (in μm) for the membrane water content varying along through-plane direction from λ = 10 to λ = 4: (a) less rigid isotropic GDL; (b) rigid isotropic GDL; (c) orthotropic GDL.

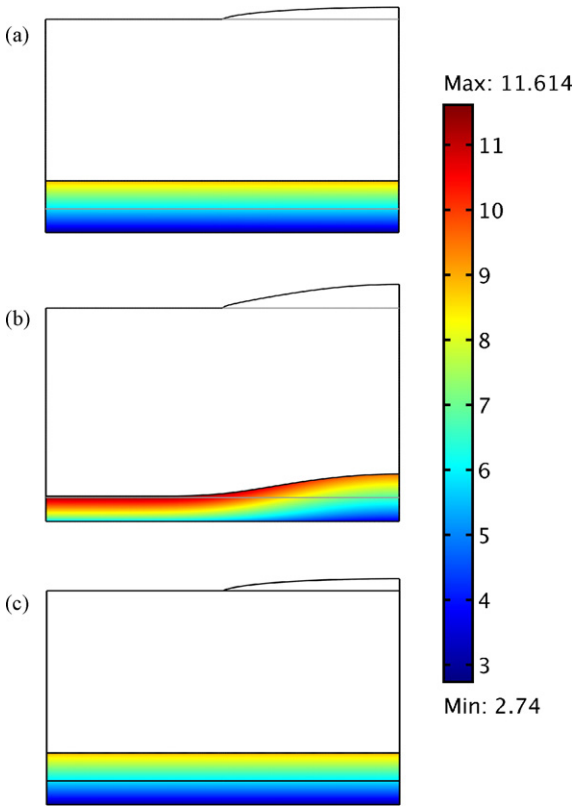

Fig. 9. In-plane compressive stress distributions (in MPa) for the membrane water content varying along through-plane direction from $\lambda = 10$ to $\lambda = 4$: (a) less rigid isotropic GDL; (b) rigid isotropic GDL; (c) orthotropic GDL.

brane. The water content profile along the vertical direction in the membrane can be seen in Fig. 5b.

Fig. 8 shows the deformations and the through-plane displacements for the same three cases we considered previously, with a water content profile that has a variation in through-plane direction. The magnitude of the maximum displacement is around 3 μm whereas it was more than 4 μm in the previous analysis when the water content gradient was in the in-plane direction. Comparing the displacements in Figs. 6c and 7c along the membrane–GDL interfaces (where the maximum displacements are seen), we see that the one in Fig. 8c is almost the average of that in Fig. 6c. As seen in Fig. 8c, the deformation is uniform at the membrane–GDL interface. For λ changing vertically the displacements are observed to be non-uniform at the same interface, the maximum displacement being at the most left end.

Another interesting observation in Fig. 8 is for the rigid isotropic GDL case (case *ii*) we observe negative displacements in the membrane. The water content is the highest at the GDL interface where the membrane tends to swell the most. However, due to the very high through-plane Young's modulus of GDL, the membrane cannot push the GDL upwards but undergoes an internal deformation (i.e. compression) resulting in negative displacements.

In Fig. 9 corresponding in-plane stress distributions are shown. For the less rigid GDL case (case *i*) and the orthotropic GDL case (case *iii*), similar distributions are observed again. The displacement fields in Fig. 8 show that in both cases the deformation of the membrane is substantially in the through-plane direction. Because of same through-plane material properties of the GDL in both cases, the compressive stress that the GDL induces on the membrane is similar to each other.

4. Conclusions

In this study we investigate the effect of the gas diffusion layer anisotropy on the mechanical behavior of the polymer electrolyte membrane of a polymer electrolyte fuel cell (PEFC) when it is subject to hygral stresses. We consider a test case to analyze the effects of GDL anisotropy, which uses a half MEA model including half of the membrane, and the GDL. The case is investigated with three different GDLs: a less rigid GDL with isotropic properties, a rigid GDL with isotropic properties and an orthotropic GDL with the actual properties. It is observed that the GDL properties have significant effect on the resultant stresses and modeling the GDL with isotropic properties leads to inaccurate predictions of the stress field. It is seen that due to very low Young's modulus of the GDL in the through-plane direction (0.5 MPa) compared to in-plane direction (9 GPa), the swelling of the membrane is almost not constrained in the through-plane direction and through-plane stresses induced in the membrane are negligible. We have also investigated the effects of non-uniform water content distribution on the stress field. Each of the in-plane and through-plane variations of the water content has a distinct effect on the deformation behavior of the membrane. Thus to produce a reliable analysis of the hygral stresses in the membrane, the water transport in the fuel cell needs to be represented rigorously.

In a companion paper [13], the development of a multi-physics modeling framework that couples the electrochemical kinetics, and transport phenomena in a PEFC with hygral stresses is shown.

Acknowledgements

We gratefully acknowledge the financial support from US Department of Energy through a cooperative research agreement DE-FG36-07GO17020 and National Science Foundation grant no. CBET-0748063 for this work.

References

[1] P. Rama, R. Chen, J. Andrews, Proc. Inst. Mech. Eng. Part A: J. Power Energy 222 (2008) 421.
[2] H. Tang, S. Peikang, S.P. Jiang, F. Wang, M. Pan, J. Power Sources 170 (2007) 85.
[3] Y. Tang, A.M. Karlsson, M.H. Santare, M. Gilbert, S. Cleghorn, W.B. Johnson, Mater. Sci. Eng. A 425 (2006) 297.
[4] Y. Tang, A. Kusoglu, A.M. Karlsson, M.H. Santare, S. Cleghorn, W.B. Johnson, J. Power Sources 175 (2008) 817.
[5] A. Webber, J. Newman, AIChE J. 50 (2004) 3215.
[6] D. Bograchev, M. Gueguen, J.C. Grandidier, S. Martemianov, Int. J. Hydrogen Energy 33 (2008) 5703.
[7] A. Kusoglu, A.M. Karlsson, M.H. Santare, S. Cleghorn, W.B. Johnson, J. Power Sources 161 (2006) 987.
[8] A. Kusoglu, A.M. Karlsson, M.H. Santare, S. Cleghorn, W.B. Johnson, J. Power Sources 170 (2007) 345.
[9] M.A.R.S. Al-Baghdadi, H.A.K.S. Al-Janabi, Int. J. Hydrogen Energy 32 (2007) 4510.
[10] Toray Carbon Paper Specification Sheet, Toray Industries Inc., Advanced Composites Department, Tokyo, 2001.
[11] U. Pasaogullari, P.P. Mukherjee, C.Y. Wang, K.S. Chen, J. Electrochem. Soc. 154 (2007) B823.
[12] J. Kleemann, F. Finsterwalder, W. Tillmetz, J. Power Sources 190 (2009) 92.
[13] M.F. Serincan, U. Pasaogullari, J. of Power Sources 196 (2011) 1303–1313.
[14] Product Information, DuPont Nafion PFSA Membranes N-112, NE-1135, N-115, N-117, NE-1110 Perfluorosulfonic Acid Polymer, NAE101, 2004.